crystals

MDPI

Article

Lanthanide Coordination Polymers as Luminescent Sensors for the Selective and Recyclable Detection of Acetone

Kaimin Wang [1], Yulu Ma [2] and Huaijun Tang [1,*]

[1] Key Laboratory of Comprehensive Utilization of Mineral Resource in Ethnic Regions, Key Laboratory of Resource Clean Conversion in Ethnic Regions, Education Department of Yunnan, School of Chemistry & Environment, Yunnan Minzu University, Kunming 650500, China; kmwang041684@163.com

[2] Key Laboratory of Medicinal Chemistry for Natural Resource Education Ministry, School of Chemical Science and Technology, Yunnan University, Kunming 650091, China; 22014000171@mail.ynu.edu.cn

* Correspondence: tanghuaijun@sohu.com; Tel.: +86-871-6591-3043

Academic Editor: Helmut Coelfen

Received: 23 May 2017; Accepted: 28 June 2017; Published: 5 July 2017

Abstract: Three new isostructural lanthanide coordination polymers {[Ln(L)$_2$·2H$_2$O]·Cl·4H$_2$O}, Ln = La (**LaL 1**), Tb (**TbL 2**), Eu (**EuL 3**), L = 4-carboxy-1-(4-carboxybenzyl)pyridinium, have been synthesized under hydrothermal conditions and characterized by single crystal X-ray diffraction, IR, TG, PXRD, and luminescence. The solid-state luminescence properties of those Ln-CPs were investigated, realizing the zwitterionic ligand (**L**) is an excellent antenna chromophore for sensitizing both Tb^{3+} and Eu^{3+} ions. We utilized **TbL 2** as a representative chemosensor to consider the potential luminescence sensing properties in different solvent suspension, which has the potential to serve as the first case of a luminescent Ln-CP material based on the zwitterionic type of organic ligand for selective and recyclable sensing of acetone in methanol solution.

Keywords: coordination polymer; crystal structure; luminescence; chemosensor; zwitterionic ligand

1. Introduction

Over the last decade, lanthanide-based metal–organic coordination polymers (Ln-CPs), as novel luminescent functional materials, have attracted a good deal of attention. They have attracted this attention not only because of their diverse architectures, but also because of their potential luminescent sensor applications for detecting cations [1,2], anions [3,4], small molecules [5], gases and vapors [6], biomolecules [7], temperature [8,9], and so on [10,11]. Compared with other luminescent sensors, Ln-CPs based luminescent sensing materials have been a rapidly developing area due to their outstanding merits such as high surface area, easily designed crystal structures, stable frameworks, and permanent porosity, as well as exposed active sites [12–14]. Recently, the zwitterionic type of organic ligands have drawn our attention [15,16], which simultaneously bear positive and negative charges with a certain separated distance on the coordination skeleton endowing special physical properties, for example, improved adsorption selectivity of gases or vapors [17]. However, to date, the Ln-CPs materials reported are usually based on the common organic ligands, while the study of Ln-CPs based on the zwitterionic types of organic ligands have rarely been reported [18]. Therefore, further systematic investigation on the Ln-CPs based on the zwitterionic types of organic ligands is absolutely necessary.

Acetone is a highly volatile organic solvent, which could stimulate cornea or metabolism disorder and have a toxic effect on the human body [19]. Considering the extensive application and potential harm of acetone, it is urgent to develop new luminescent sensors to detect it. To date, only a few CPs

have been reported for the sensing of acetone [20–23], most of which were constructed by d^{10} transition metal ions (Zn and Cd) and π-conjugated ligands, whereas coordination polymer materials based on lanthanide ions have been rarely published [24]. The advantages of those lanthanide materials over the transition metal luminescent materials include the sharp and strong emissions, large stokes shifts, high quantum yields, and long luminescence lifetimes, which originate from f–f transitions of lanthanide ions [25]. Taking into account these kinds of sensor materials are still defective, the synthesis and development of new materials based on lanthanide CPs for fluorescent high selective detection of acetones is still a major challenge.

As an effective combination of the above mentioned aspects, we selected the zwitterionic types of organic ligand 4-carboxy-1-(4-carboxybenzyl)pyridinium chloride (H_2LCl) as ligand to construct three isostructrual lanthanide coordination polymers {[Ln(L)$_2$·2H$_2$O]·Cl·4H$_2$O}, Ln = La (**LaL 1**), Tb (**TbL 2**), Eu (**EuL 3**). Those materials have the potential to serve as the first example of a luminescent Ln-CP material based on the zwitterionic type of organic ligand for selective and recyclable sensing of acetone in methanol solution.

2. Results

2.1. Crystal Structures

2.1.1. Descriptions of the Crystal Structures of {[La(L)$_2$·2H$_2$O]·Cl·4H$_2$O} (**1**)

The X-ray single-crystal diffraction studies reveal that compound **LaL 1** crystallizes in the *P*$\bar{1}$ space group of the triclinic system. As shown in Figure 1a, each La^{3+} center is eight-coordinated by six oxygen atoms (O1, O5, O8A, O4C, O2B, and O3D) from different L ligands and two oxygen atoms (O9 and O10) from two coordinated water molecules. The asymmetric unit of **LaL 1** contains one crystallographically independent La^{3+}, two deprotonated L ligands, two coordinated water molecules, one free Cl^- ion, and four guest water molecules. There are two kinds of coordination modes for the two carboxylate groups of L ligand; one adopts bidentate bridging coordination fashion μ_2-$\eta^1\eta^1$ and the other one shows monodentate bridging coordination mode μ_1-η^1. The two adjacent La^{3+} ions are connected together through four carboxylate groups of four L ligands in bidentate bridging coordination mode to form a dinuclear unit (Figure 1), then neighboring dinuclear subunits are bridged by these four L ligands in opposite direction to form 1D beaded chain. When adjacent, these chains are further connected by other 1D beaded chains, building by L ligands in unidentate bridging coordination mode, to form a 2D network (Figure 1). The angle between these two chains is 78.71°. The 3D supramolecular architecture of compound **LaL 1** is obtained from the interlayer π···π stacking interactions between neighboring phenyl rings and benzene rings in adjacent layers (centroid−centroid: 3.534(2) Å, 3.888(3) Å and 3.623(2) Å). (Figure 1)

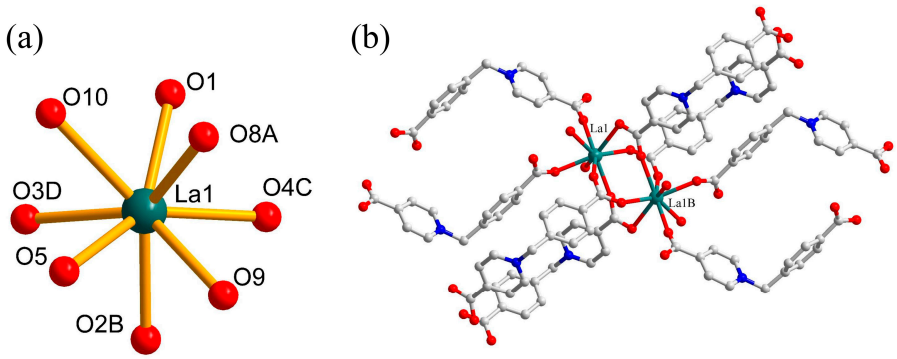

Figure 1. *Cont.*

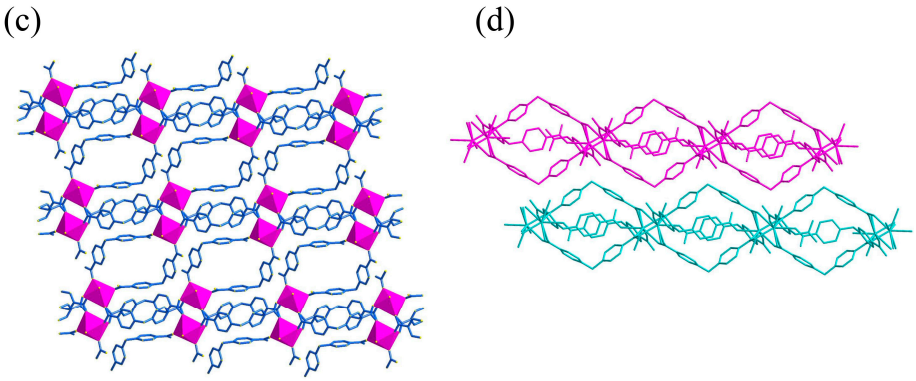

Figure 1. (**a**) Coordination environment of the La^{3+} ion center. Symmetry codes: (A) A –x + 1, −y + 1, −z + 1; (B) –x + 2, -y + 2, −z + 2; (C) –x + 1, −y + 1, −z + 2; (D) x + 1, y + 1, z. (**b**) Two adjacent La^{3+} ions are bridged by four carboxylate groups from four L ligands. (**c**) 2D network of compound **1**. (**d**) 3D supramolecular structure of compound **1**.

2.1.2. PXRD Analysis

To determine whether the crystal structures are truly representative of the bulk materials tested in property studies, powder X-ray diffraction (PXRD) experiments were carried out for compounds **1**–**3**. The PXRD experimental and as-simulated patterns of compounds **1**–**3** are shown in the Figure 2. Failing to obtain crystals suitable for single-crystal crystallography, we were unable to determine the structures of **TbL 2** and **EuL 3**, but the PXRD patterns of **TbL 2** and **EuL 3** are in good agreement with that of **LaL 1**, with only minor shifts in peak positions, indicating that **TbL 2** and **EuL 3** are isomorphous with **LaL 1**, and indicating that the crystal structures are truly representative of the bulk crystal products. The differences in intensity may be owing to the preferred orientation of the crystal samples.

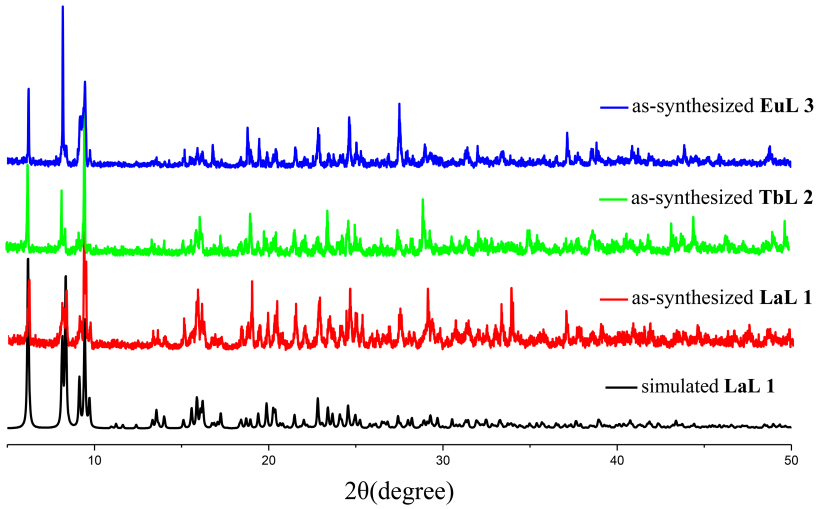

Figure 2. The PXRD patterns of **LaL 1**, **TbL 2**, **EuL 3**.

*2.2. Solid-State Luminescence of **1**–**3***

The solid-state luminescence properties and the excitation spectrum of the H_2LCl ligand and compounds **1**–**3** were recorded at room temperature as shown in Figure 3 and Figure S1, respectively. As shown in Figure 3, complex **LaL 1** presents a broad emission band centered at 409 nm (λ_{ex} = 332 nm), which is assigned to the typical π^*–π transition of ligands (Figure 3). The blue shift compared to the

ligand emission is presumably due to a conformational change in the ligand upon binding with the metal ions [20–23]. Upon excitation at 332 nm, complex **TbL 2** showed four characteristic emission bands of Tb^{3+} ion, centered at 489, 544, 582, and 619 nm (Figure 3), and these emissions are attributed to the f–f electronic transitions $^5D_4 \rightarrow {}^7F_J$ (J = 6, 5, 4 and 3), respectively. Among these transitions, $^5D_4 \rightarrow {}^7F_5$ (544 nm) green emission is a dominating intensity. While being excited at 332 nm, complex **EuL 3** displays emissions at 590, 613, and 653 nm, which are attributed to the $^5D_0 \rightarrow {}^7F_J$ (J = 1, 2, and 3) transitions of the Eu^{3+} ion, with a maximum at $^5D_0 \rightarrow {}^7F_2$ transition (613 nm) (Figure 3). Notably, there was no emission band of the ligand observed in the emission spectra of the compounds, indicating efficient energy transfer from the ligand to the Tb^{3+} ion or Eu^{3+} ion. These results clearly indicate that the L ligand is an excellent antenna chromophore for sensitizing both Tb^{3+} and Eu^{3+} ions.

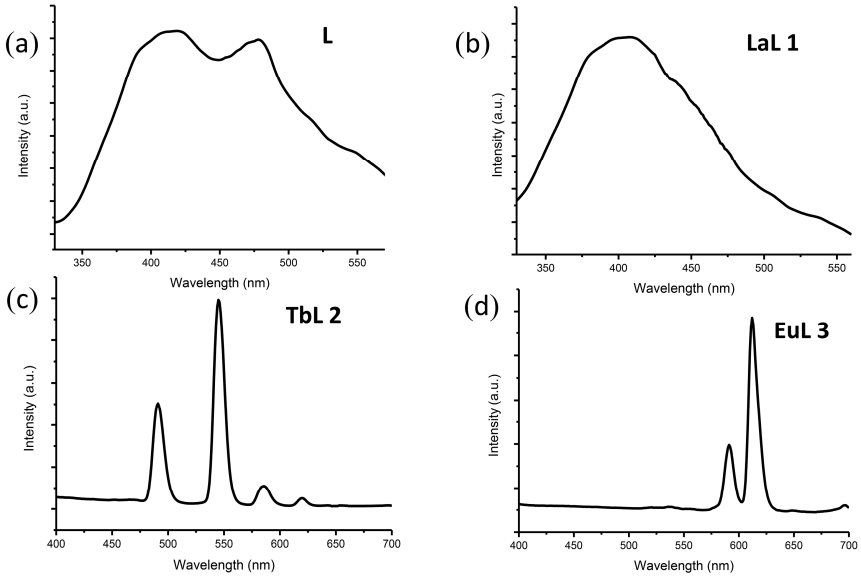

Figure 3. The solid-state emisssion spectra of (**a**) the H_2LCl ligand with λ_{ex} = 302 nm, (**b**) **LaL 1**, with λ_{ex} = 332 nm, (**c**) **TbL 2** with λ_{ex} = 332 nm, (**d**) **EuL 3** with λ_{ex} = 332 nm.

2.3. Organic Small Molecule Sensing

The high luminescence intensities of those CPs prompt us to utilize **TbL 2** as a representative to consider the potential luminescence sensing properties in different solvent suspension. Firstly, the finely ground sample of **TbL 2** (10 mg) is immersed in different common organic solvents (5 mL), treated by ultrasonication for 60 min, and then aged for 24 h to generate stable suspensions before the fluorescence study. The solvents used are methanol, trichloromethane, tetrahydrofuran, dichloromethane, cyclohexane, *n*-hexane, acetonitrile (CH_3CN), *N*,*N*-dimethylacetamide (DMA), *N*,*N*-dimethylformamide (DMF), and acetone. Interestingly, the most interesting feature is that its luminescent emission spectrum, monitored at 613 nm ($^5D_4 \rightarrow {}^7F_3$), is largely dependent on the solvent molecules, particularly in the case of acetone, which exhibit the most significant quenching effects (Figure 4). Such solvent-dependent luminescence properties are of interest for the sensing of acetone solvent molecules. To explain the reason for the quenching effect, the absorption spectra of methanol and acetone are investigated, which reveals that acetone has a wide absorption range from 308 to 360 nm, while methanol exhibits no absorption (Figure S2). The absorbing band of acetone overlays part of the absorption band of sensor **TbL 2**, which may lead to energy transfer occuring between the sensor **TbL 2** and the acetone molecules. Due to the intermolecular solute-solvent interactions between **TbL 2** and acetone, the energy absorbed by **TbL 2** is transferred to acetone molecules, resulting in a decrease in the luminescent intensity, which is similar to the previously reported CP-based sensors [22,23].

For better understanding of the sensing ability of **TbL 2** for acetone, the sensing properties of **TbL 2** for acetone were also investigated by recording the emissive spectra of the **2**-methanol suspension with the gradual addition of acetone. As shown in Figure 4, the luminescence intensity monitored at 613 nm decreases clearly with the increasing acetone concentration. Moreover, the quenching effect can be rationalized for the low concentrations by the Stern–Volmer equation: $I_o/I = 1 + K_{sv} \times [M]$, where I_o and I are the luminescence intensities of ethanol suspensions of complex **TbL 2** before and after the addition of acetone, respectively; K_{sv} is the quenching constant, and [M] is the molar concentration of acetone [20–24]. On the basis of the quenching experimental data, the linear correlation coefficient (R^2) in the K_{sv} curve of **TbL 2** with addition of acetone is 0.9877 (Figure 4), suggesting that the quenching effect of TNP on the fluorescence of **TbL 2** fits well the Stern–Volmer model. The K_{sv} is 2.0263 $\times$ 10^4 M^{-1} at low concentrations of acetone, which is comparable to those of previously reported CP-based sensors [20–24].

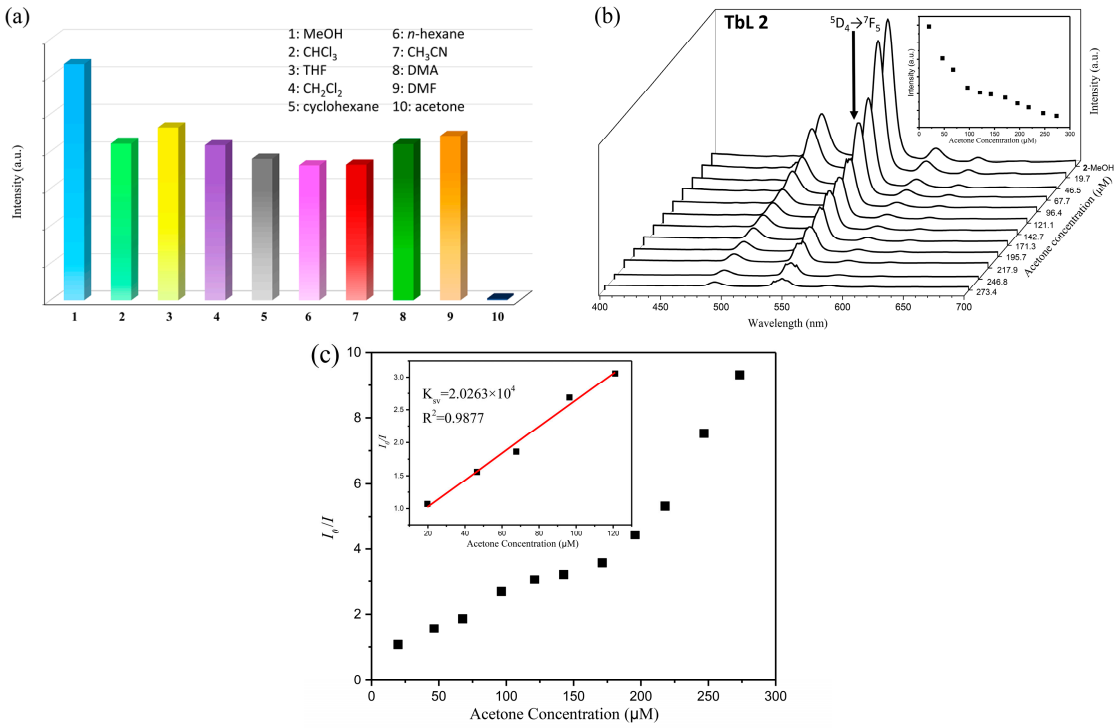

Figure 4. (**a**) Comparisons of the luminescence intensity of **TbL 2** in different solvent suspensions at room temperature (λ_{ex} = 332 nm). (**b**) The luminescence emission spectra titration of **TbL 2**-dispersed in methanol with the addition of different concentrations of acetone at room temperature (λ_{ex} = 332 nm). (**c**) Stern–Volmer plot of I_o/I versus the concentration of acetone in the **2**-menthanol suspension (insert: enlarged view of a selected area).

Additionally, we also found that **TbL 2** can be regenerated and reused for five numbers of cycles by centrifuging the dispersed crystals in methanol after sensing and washing several times with methanol (Figure 5). The quenching efficiencies of every cycle are basically unchanged through monitoring the emission spectra of **TbL 2** dispersed in the presence of 200 μM acetone in methanol. Furthermore, the PXRD patterns of the initial sample and recovered by centrifuging of the dispersed crystals in methanol after sensing and washing several times with methanol indicate the high stability of this compound (Figure S3). The result reveals that **TbL 2** could be applied as a fluorescence sensor for acetone with high selectivity and recyclability.

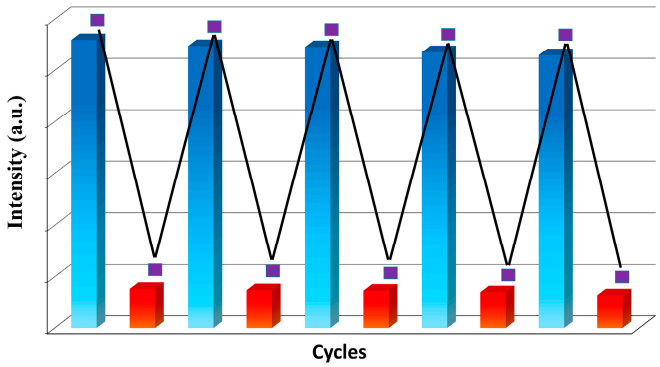

Figure 5. The quenching and recyclability test of **TbL 2** upon addition of 200 μM acetone in methanol solution. The luminescence was recovered by centrifuging the dispersed crystals in methanol after sensing and washing several times with methanol.

3. Experimental Section

CCDC 1498357 (**1**) contains the supplementary crystallographic data for this paper. This data can be obtained free of charge from the Cambridge Crystallographic Data Center via the internet at http://www.ccdc.cam.ac.uk/data_request/cif, or by e-mailing data_request@ccdc.cam.ac.uk.

3.1. Material and Methods

All of the reagents and solvents used in this paper were purchased from Adamas-beta Co., Ltd. (Shanghai, China) and used as received without further purification, unless otherwise indicated. The NMR spectra were recorded on a Bruker DRX400 (^{1}H: 400 MH$_Z$, ^{13}C: 100 MH$_Z$), chemical shifts (δ) are expressed in ppm, and *J* values are given in Hz, and deuterated DMSO was used as solvent. IR spectra were recorded on a FT-IR Thermo Nicolet Avatar 360 using KBr pellet. The phase purity of the samples was investigated by powder X-ray diffraction (PXRD) measurements carried out on a Bruker D8-Advance diffractometer equipped with CuKα radiation (λ = 1.5406 Å) at a scan speed of 1°/min. Thermal stability studies were carried out on a NETSCHZ STA-449C thermoanalyzer with a heating rate of 10 °C/min under a nitrogen atmosphere. All fluorescence measurements were performed on an Edinburgh Instrument F920 spectrometer. C, H, and N were determined on an Elementar Vario III EL elemental analyzer.

3.2. Synthetic Procedures

3.2.1. Synthesis of 4-Carboxy-1-(4-Carboxybenzyl)Pyridinium Chloride (H_2LCl)

A mixture of isonicotinic acid (1.231 g, 10 mmol) and methyl 4-(bromomethyl)benzoate (2.291 g, 10 mmol) in CH_3CN (50 mL) was refluxed for 8 h. After the mixture was cooled down to room temperature, the resulting precipitate was filtered to provide a white solid which was dissolved and refluxed in 100 mL 2 N HCl aqueous solution for 2 h. After the solution cooled down to ambient temperature, the white precipitate formed were collected by filtration and washed with ether (20 mL × 3) to afford H_2LCl (2.712 g, 92%) which was identical to data in the literature [15,26]. ^{1}H NMR (400 Hz, DMSO-*d*6): δ = 9.46 (d, 2H, ArH, *J* = 6.4 Hz), 8.52 (d, 2H, ArH, *J*= 6.4 Hz), 7.99 (d, 2H, ArH, *J* = 8.4 Hz), 7.67 (d, 2H, ArH, *J* = 8.4 Hz), 6.12 (s, 2H, CH_2); ^{13}C NMR (100 Hz, DMSO-*d*6): δ = 167.2, 163.8, 146.9, 146.5, 139.0, 132.1, 130.45, 129.5, 128.2, 63.2. (Figure S4).

3.2.2. Synthesis of {[La(L)$_2$·2H_2O]·Cl·4H_2O} (**LaL 1**)

$LaCl_3$·6H_2O (0.3 mmol), H_2LCl (0.1 mmol), NaOH (0.2 mmol) and H_2O (10 mL) were added to a 15 mL Telfon-lined stainless steel autoclave, and the solution was heated at 150 °C for 24 h, then cooled down to room temperature at a rate of 2 °C/h. Colorless block crystals of the product were

collected by filtration and washed with water several times, then dried in air. The obtained yield based on the H_2LCl was 22.5%. Main IR (KBr, cm^{-1}): 3382, 3113, 3051, 1621, 1540, 1397, 1172, 1131 (Figure S5). The TG curve for **LaL 1** shows a gradual weight loss 13.8% between 90 and 280 °C, which can be ascribed to the removal of two lattice water molecules and four free water molecules (Figure S6). The phase purity of the product was confirmed by PXRD experiments (Figure 2). Anal. Calcd for $C_{28}H_{32}ClLaN_2O_8$ (698.9337): C, 48.12; H, 4.61; N, 4.01. Found: C, 48.05; H, 4.69; N, 3.98.

3.2.3. Synthesis of {[Tb(L)$_2$·2H$_2$O]·Cl·4H$_2$O} (**TbL 2**)

All attempts to get single crystals of **TbL 2** by different methods were in vain. The procedure was similar to that of complex **LaL 1** except that $TbCl_3·6H_2O$ was used instead of $LaCl_3·6H_2O$. Yield: 19.2% (based on the ligand). The phase purity of the product was confirmed by PXRD experiments (Figure 2). Main IR (KBr, cm^{-1}): 3395, 3113, 3047, 1625, 1544, 1397, 1176, 1131. (Figure S5). Anal. Calcd for $C_{28}H_{32}ClN_2O_8Tb$ (718.9437): C, 46.78; H, 4.49; N, 3.90. Found: C, 46.71; H, 4.53; N, 3.87.

3.2.4. Synthesis of {[Eu(L)$_2$·2H$_2$O]·Cl·4H$_2$O} (**EuL 3**)

All attempts to get single crystals of **EuL 3** by different methods were in vain. The procedure was similar to that of complex **LaL 1** except that $EuCl_3·6H_2O$ was used instead of $LaCl_3·6H_2O$. Colorless precipitates were isolated in a yield of 13.5% (based on the ligand). The phase purity of the product was confirmed by PXRD experiments (Figure 5). Main IR (KBr, cm^{-1}): 3391, 3109, 3051, 1621, 1548, 1397, 1176, 1131. (Figure S5). Anal. Calcd for $C_{28}H_{32}ClEuN_2O_8$ (711.9837): C, 47.24; H, 4.53; N, 3.93. Found: C, 47.19; H, 4.58; N, 3.91.

3.3. Crystallography

Crystallographic data were collected at 296 K on a Bruker Smart AXS CCD diffractometer with graphite-monochromated Mo Kα radiation (λ = 0.71073 Å) using ω-scan technique. Cell parameters were retrieved using SMART software and refined with SAINT on all observed reflections. Absorption corrections were applied with the program SADABS. Structure **LaL 1** was solved by direct methods using SHELXS-97 [27] and refined on F2 by full-matrix least-squares procedures with SHELXL-97 [28]. All nonhydrogen atoms were located in different Fourier syntheses and finally refined with anisotropic displacement parameters. Hydrogen atoms attached to the organic moieties were either located from the difference Fourier map or fixed stereochemically. The final chemical formula was estimated and combined with the TGA results. Details of the crystallographic data collection and refinement parameters are summarized in Table 1. Main bond lengths and angles are presented in Table 2.

Table 1. Crystal data and structure refinement for **1**.

Compound	1
Chemical formula	$C_{28}H_{32}N_2O_{14}ClLa$
Formula mass	794.92
Crystal system	Triclinic
a/Å	11.3001(7)
b/Å	11.7346(7)
c/Å	14.6280(9)
α/°	100.2340(10)
β/°	93.7830(10)
γ/°	109.1450(10)
Unit cell volume/Å^3	1787.09(19)
Space group	$P\bar{1}$
Z	2
D_X/Mg m^{-3}	1.343
μ/mm^{-1}	1.318

Table 1. *Cont.*

Compound	**1**
Reflections with $I > 2\sigma(I)$	7215
Independent reflections	8114
F(000)	720
R_{int}	0.0245
GOF on F^2	1.094
R_1, wR_2 [$I > 2\sigma(I)$]	0.0327, 0.0955
R_1, wR_2 [all data]	0.0375, 0.1000
Residuals/e Å^{-3}	0.793, −0.638
CCDC number	1498357

Table 2. Elected bond lengths (Å) and angles (°) for compound **1**.

Bond lengths (Å) for **1**			
La(1)-O(5)	2.448(3)	O(2)-C(6)	1.254(4)
La(1)-O(8)A	2.490(3)	O(3)-C(14)	1.246(4)
La(1)-O(1)	2.504(3)	O(4)-C(14)	1.260(4)
La(1)-O(2)B	2.508(3)	O(5)-C(20)	1.237(5)
La(1)-O(4)C	2.512(2)	O(6)-C(20)	1.252(6)
La(1)-O(3)D	2.562(2)	O(7)-C(28)	1.247(5)
La(1)-O(10)	2.569(3)	O(8)-C(28)	1.269(5)
La(1)-O(9)	2.605(3)	N(1)-C(4)	1.356(5)
La(1)-O(4)D	2.959(2)	N(1)-C(3)	1.380(5)
O(1)-C(6)	1.244(4)	N(1)-C(7)	1.502(4)
Bond angles (°) for **1**			
O(5)-La(1)-O(8)A	91.37(11)	O(3)D-La(1)-O(10)	68.16(9)
O(5)-La(1)-O(1)	145.38(9)	O(5)-La(1)-O(9)	71.04(10)
O(8)A-La(1)-O(1)	79.47(10)	O(8)A-La(1)-O(9)	69.88(10)
O(5)-La(1)-O(2)B	79.90(9)	O(1)-La(1)-O(9)	133.44(9)
O(8)A-La(1)-O(2)B	139.19(10)	O(2)B-La(1)-O(9)	69.58(10)
O(1)-La(1)-O(2)B	127.76(9)	O(4)C-La(1)-O(9)	75.85(9)
O(5)-La(1)-O(4)C	144.80(9)	O(3)D-La(1)-O(9)	138.14(10)
O(8)A-La(1)-O(4)C	88.20(9)	O(10)-La(1)-O(9)	127.61(10)
O(1)-La(1)-O(4)C	68.85(8)	O(5)-La(1)-O(4)D	119.81(9)
O(2)B-La(1)-O(4)C	77.69(9)	O(8)A-La(1)-O(4)D	146.12(9)
O(5)-La(1)-O(3)D	79.70(9)	O(1)-La(1)-O(4)D	67.36(8)
O(8)A-La(1)-O(3)D	141.40(9)	O(2)B-La(1)-O(4)D	65.49(8)
O(1)-La(1)-O(3)D	86.90(9)	O(4)C-La(1)-O(4)D	73.97(8)
O(2)B-La(1)-O(3)D	76.46(9)	O(3)D-La(1)-O(4)D	46.25(7)
O(4)C-La(1)-O(3)D	120.19(8)	O(10)-La(1)-O(4)D	101.20(8)
O(5)-La(1)-O(10)	74.02(10)	O(9)-La(1)-O(4)D	129.85(9)
O(8)A-La(1)-O(10)	73.27(9)	C(6)-O(1)-La(1)	139.4(2)
O(1)-La(1)-O(10)	71.36(9)	C(6)-O(2)-La(1)B	136.0(2)
O(2)B-La(1)-O(10)	138.94(10)	C(4)-N(1)-C(3)	120.5(3)
O(4)C-La(1)-O(10)	138.48(9)	C(4)-N(1)-C(7)	119.4(3)
O(3)D-La(1)-O(10)	68.16(9)	C(3)-N(1)-C(7)	120.1(3)

4. Conclusions

In summary, we have designed three isostructural lanthanide coordination polymers (Ln-CPs) to explore chemosensors. Firstly, the solid-state luminescence properties of those Ln-CPs were investigated, realizing the zwitterionic ligand (L) is an excellent antenna chromophore for sensitizing both Tb^{3+} and Eu^{3+} ions. In addition, **TbL 2** as a representative chemosensor, material could not only serve as a chemosensor for acetone but also can be regenerated and reused for at least five cycles. Owing to a few luminescent CP, sensors for detecting acetone have been realized and reported [20–23], to the best of our knowledge, those materials have the potential to serve as the first case of a luminescent

Ln-CP material based on the zwitterionic type of organic ligand for selective and recyclable sensing of acetone in methanol solution. Further studies are under way in our lab.

Supplementary Materials: The following are available online at www.mdpi.com/2073-4352/7/7/199/s1. Figure S1: The solid-state excitation spectra of ligand H_2LCl, complex **1**, **2**, and **3**. Figure S2: The UV/Vis absorption spectra for acetone and methanol. Figure S3: PXRD patterns of **1** after detection of acetone (after five cycles reused). Figure S4: ^{1}H NMR (400 Hz, DMSO-*d*6) and ^{13}C NMR (100 Hz, DMSO-*d*6) spectra of H_2LCl Ligand. Figure S5: The IR spectra of ligand H_2LCl, complex **1**, **2**, and **3**. Figure S6: The TGA diagram of **1** as a representative.

Acknowledgments: This work was supported by the Yunnan Provincial Department of Education funded projects (2017ZZX085), the National Natural Science Foundation of China (Projects 21371151) and the Yunnan Province doctoral newcomer Award (YN2015015 and YN2014017).

Author Contributions: Kaimin Wang designed the experiments and wrote the paper; Yulu Ma carried out the synthesis experiments; Huaijun Tang performed X-ray structure determination and Yulu Ma analyzed the results; Huaijun Tang performed X-ray powder diffraction analysis; Yulu Ma performed the other experiments. All authors took part in the discussion processes and have approved the final manuscript.

Conflicts of Interest: The authors declare no conflict of interest.

References

1. Jin, J.-C.; Wu, J.; Yang, G.-P.; Wu, Y.-L.; Wang, Y.-Y. A microporous anionic metal–organic framework for a highly selective and sensitive electrochemical sensor of Cu^{2+} ions. *Chem. Commun.* **2016**, *52*, 8475–8478. [CrossRef] [PubMed]
2. Hu, Z.; Deibert, B.J.; Li, J. Luminescent metal–organic frameworks for chemical sensing and explosive detection. *Chem. Soc. Rev.* **2014**, *43*, 5815–5840. [CrossRef] [PubMed]
3. Cao, C.-S.; Hu, H.-C.; Xu, H.; Qiao, W.-Z.; Zhao, B. Two solvent-stable MOFs as a recyclable luminescent probe for detecting dichromate or chromate anions. *CrystEngComm* **2016**, *18*, 4445–4451. [CrossRef]
4. Chen, B.; Wang, L.; Zapata, F.; Qian, G.; Lobkovsky, E.B. A Luminescent Microporous Metal−Organic Framework for the Recognition and Sensing of Anions. *J. Am. Chem. Soc.* **2008**, *130*, 6718–6719. [CrossRef] [PubMed]
5. Shi, N.; Zhang, Y.; Xu, D.; Song, C.; Jin, X.; Liu, D.; Xie, L.; Huang, W. π-System based coordination polymer hollow nanospheres for the selective sensing of aromatic nitro explosive compounds. *New J. Chem.* **2015**, *39*, 9275–9280. [CrossRef]
6. Barea, E.; Montoro, C.; Navarro, J.A.R. Toxic gas removal—metal–organic frameworks for the capture and degradation of toxic gases and vapours. *Chem. Soc. Rev.* **2014**, *43*, 5419–5430. [CrossRef] [PubMed]
7. Qin, L.; Lin, L.-X.; Fang, Z.-P.; Yang, S.-P.; Qiu, G.-H.; Chen, J.-X.; Chen, W.-H. A water-stable metal–organic framework of a zwitterionic carboxylate with dysprosium: A sensing platform for Ebolavirus RNA sequences. *Chem. Commun.* **2016**, *52*, 132–135. [CrossRef] [PubMed]
8. Shen, X.; Yan, B. Polymer hybrid thin films based on rare earth ion-functionalized MOF: Photoluminescence tuning and sensing as a thermometer. *Dalton Trans.* **2015**, *44*, 1875–1881. [CrossRef] [PubMed]
9. Du, P.-Y.; Gu, W.; Liu, X. Highly selective luminescence sensing of nitrite and benzaldehyde based on 3d–4f heterometallic metal–organic frameworks. *Dalton Trans.* **2016**, *45*, 8700–8704. [CrossRef] [PubMed]
10. Xu, Z.-X.; Ma, Y.-L.; Zhang, L.-S.; Zhang, J. A couple of Co(II) enantiomers constructed from semirigid lactic acid derivatives. *Inorg. Chem. Commum.* **2016**, *73*, 115–118. [CrossRef]
11. Xu, Z.-X.; Ma, Y.-L.; Lv, G.-L. Homochiral coordination polymers with helixes and metal clusters based on lactate derivatives. *J. Solid State Chem.* **2017**, *249*, 210–214. [CrossRef]
12. Suckert, S.; Germann, L.S.; Dinnebier, R.E.; Werner, J.; Näther, C. Synthesis, Structures and Properties of Cobalt Thiocyanate Coordination Compounds with 4-(hydroxymethyl)pyridine as Co-ligand. *Crystals* **2016**, *6*, 38. [CrossRef]
13. Semitut, E.; Komarov, V.; Sukhikh, T.; Filatov, E.; Potapov, A. Synthesis, Crystal Structure and Thermal Stability of 1D Linear Silver(I) Coordination Polymers with 1,1,2,2-Tetra(pyrazol-1-yl)ethane. *Crystals* **2016**, *6*, 138. [CrossRef]
14. Nakanishi, T.; Sato, O. Synthesis, Structure, and Magnetic Properties of New Spin Crossover Fe(II) Complexes Forming Short Hydrogen Bonds with Substituted Dicarboxylic Acids. *Crystals* **2016**, *6*, 131. [CrossRef]

15. Wang, K.-M.; Du, L.; Ma, Y.-L.; Zhao, J.-S.; Wang, Q.; Yan, T.; Zhao, Q.-H. Multifunctional chemical sensors and luminescent thermometers based on lanthanide metal–organic framework materials. *CrystEngComm* **2016**, *18*, 2690–2700. [CrossRef]
16. Ma, Y.; Du, L.; Wang, K.; Zhao, Q. Synthesis, Crystal Structure, Luminescence and Magnetism of Three Novel Coordination Polymers Based on Flexible Multicarboxylate Zwitterionic Ligand. *Crystals* **2017**, *7*, 32. [CrossRef]
17. Pan, M.; Du, B.-B.; Zhu, Y.-X.; Yue, M.-Q.; Wei, Z.-W.; Su, C.-Y. Highly Efficient Visible-to-NIR Luminescence of Lanthanide (III) Complexes with Zwitterionic Ligands Bearing Charge-Transfer Character: Beyond Triplet Sensitization. *Chem. Eur. J.* **2016**, *22*, 2440–2451. [CrossRef] [PubMed]
18. Wen, R.-M.; Han, S.-D.; Ren, G.-J.; Chang, Z.; Li, Y.-W.; Bu, X.-H. A flexible zwitterion ligand based lanthanide metal–organic framework for luminescence sensing of metal ions and small molecules. *Dalton Trans.* **2015**, *44*, 10914–10917. [CrossRef] [PubMed]
19. Li, Y.; Song, H.; Chen, Q.; Liu, K.; Zhao, F.-Y.; Ruan, W.-J.; Chang, Z. Two coordination polymers with enhanced ligand-centered luminescence and assembly imparted sensing ability for acetone. *J. Mater. Chem. A* **2014**, *2*, 9469–9473. [CrossRef]
20. Shi, Y.-X.; Hu, F.-L.; Zhang, W.-H.; Lang, J.-P. A unique Zn (II)-based MOF fluorescent probe for the dual detection of nitroaromatics and ketones in water. *CrystEngComm* **2015**, *17*, 9404–9412. [CrossRef]
21. Hua, J.-A.; Zhao, Y.; Kang, Y.-S.; Lu, Y.; Sun, W.-Y. Solvent-dependent zinc (II) coordination polymers with mixed ligands: selective sorption and fluorescence sensing. *Dalton Trans.* **2015**, *44*, 11524–11532. [CrossRef] [PubMed]
22. Gu, F.; Chen, H.; Han, D.; Wang, Z. Metal–organic framework derived Au@ ZnO yolk–shell nanostructures and their highly sensitive detection of acetone. *RSC Adv.* **2016**, *6*, 29727–29733. [CrossRef]
23. Liu, X.-J.; Zhang, Y.-H.; Chang, Z.; Li, A.-L.; Tian, D.; Yao, Z.-Q.; Jia, Y.-Y.; Bu, X.-H. A Water-Stable Metal–Organic Framework with a Double-Helical Structure for Fluorescent Sensing. *Inorg. Chem.* **2016**, *55*, 7326–7328. [CrossRef] [PubMed]
24. Hao, J.-N.; Yan, B. Ln^{3+} post-functionalized metal–organic frameworks for color tunable emission and highly sensitive sensing of toxic anions and small molecules. *New J. Chem.* **2016**, *40*, 4654–4661. [CrossRef]
25. Barry, D.E.; Caffrey, D.F.; Gunnlaugsson, T. Lanthanide-directed synthesis of luminescent self-assembly supramolecular structures and mechanically bonded systems from acyclic coordinating organic ligands. *Chem. Soc. Rev.* **2016**, *45*, 3244–3274. [CrossRef] [PubMed]
26. Zhang, J.-Y.; Wang, K.; Li, X.-B.; Gao, E.-Q. Magnetic coupling and slow relaxation of magnetization in chain-based MnII, CoII, and NiII coordination frameworks. *Inorg. Chem.* **2014**, *53*, 9306–9314. [CrossRef] [PubMed]
27. Sheldrick, G.M. *SHELXS-97, Program for the Solution of Crystal Structures*; University of Göttingen: Göttingen, Germany, 1997.
28. Sheldrick, G.M. A short history of SHELX. *Acta Crystallogr. Sect. A* **2008**, *64*, 112–122. [CrossRef] [PubMed]